Thermal performance measurements on ATLAS-SCT KB forward modules

M. Donegà [a 1], A. Clark [a], M. D'Onofrio [a], D. Ferrere [a], C. Hirt [a], Y. Ikegami [c], T. Kohriki [c], T. Kondo [c], S. Lindsay [d], M. Mangin-Brinet [a], T. Niinikoski [b], H. Pernegger [b], E. Perrin [a], G. Taylor [d], S. Terada [c], Y. Unno [c], R. Wallny [b], M. Weber [a]

[a] *Univérsite de Genève*

[b] *CERN (European Council for Nuclear Research)*

[c] *KEK, Japan*

[d] *University of Melbourne*

Abstract

The thermal design of the KB module is presented. A Finite Elements Analysis (FEA) has been used to finalize the module design. The thermal performance of an outer irradiated KB module has been measured at different cooling conditions. The thermal runaway of the module has been measured. The FEA model has been compared with the measurements and has been used to predict the thermal performance in a realistic SCT scenario.

[1] *Email address:* mauro.donega@cern.ch

16 May 2003

Contents

1 Introduction

During 2001 the ATLAS-SCT endcap module community was facing a crisis. The outer and middle forward modules based on K4 (Kapton) hybrids showed electrical instabilities. [2] On the other hand the barrel modules equipped with the same readout chips, did not show such a pronounced problem.

At that time there were many open questions on where the problem could be localized. Electrical tests on inner (shorter strips) modules showed that they were less affected by instabilities. In order to better understand the problem, two parallel paths were studied: to improve the existing endcap hybrid, including new grounding planes, or to prototype an endcap outer module with a barrel hybrid (the backup solution). The name of this project was KB (Kapton and Barrel). Since the hybrid has a different geometry, a completely new mechanical and thermal design for the module layout was developed.

2 Thermal Performance Specifications

All the modules of the SCT (ATLAS Silicon Tracker) have to meet mechanical, thermal and electrical specifications in order to assure that the system works efficiently and reliably. The thermal specifications are described in reference [1]. The module will operate in a nitrogen (N_2) atmosphere and it is estimated that it will receive from the environment at most an additional heat load of ∼0.2 W per detector, coming from radiation and convection. The inner module, having only two detectors, will collect ∼0.4 W from the environment, while the outer and middle modules, with four detectors, will collect ∼0.8 W.
The thermal specifications can be summarized as follows:

- when the module is dissipating 7 W on the read-out electronics, 185 $\mu W/\mathrm{mm}^2$ at 0 °C on the detectors and is subjected to the environment heat load, the detectors should be cooler than -7 °C
- when the power on the hybrid is 7 W and the module is charged with the environmental heat load, thermal runaway must not occur unless the detector power density is above 240 $\mu W/\mathrm{mm}^2$ at 0 °C .

The first specification aims at reducing the electronic noise and getting the most favorable annealing condition. The second specifications sets a strict limit on the thermal runaway. The detector leakage current is temperature dependent, following the equation:

$$I_{leak}(T) \propto T^2 e^{\frac{-E_g}{2K_B T}} \tag{1}$$

[2] The readout electronics of the ATLAS-SCT modules is binary. The charge collected by the strips is amplified and then goes through a discriminator. If the charge is above a fixed threshold, commonly 1 fC, the electronics produces a logic-level 1 signal. The stability of a fixed reference value for the discriminator (the grounding), dictates the reliability of the outputs, and fluctuations in this reference translates into a so called module instability.

where T is the temperature on the detectors, E_g is the effective charge carrier activation energy of the silicon after irradiation ($\sim$1.2 eV) and K_B is the Boltzmann constant. The power dissipated by the detectors increases their temperature and so the leakage current increases, that in turn increases the power dissipation. If the cooling system is able to remove the power dissipated by the detectors, this loop will reach a stable condition; if not, it will diverge in an unstable condition commonly called *thermal runaway*. Since the thermal runaway represents a dramatic failure of the module that will oblige the user to switch the module off, the specification on it is very restrictive and requires the module to be able to stand 30% more than the maximal expected power density on the detectors before failing.

3 Thermal Simulations

The first studies on possible geometries of the module were performed using thermal FEA (Finite Element Analysis) studies. Only when the design looked satisfactory was a prototype module built and tested.

3.1 Thermal design concept

According to their radial position on the disk there are three types of endcap modules: inner, middle and outer. The inner module is the shortest module with one microstrip detector per side, while middle and outer modules have two detectors per side.
The baseline cooling design relies on two cooling points: a main cooling block removing the heat dissipated by the hybrid and the heat generated by the detectors and a second cooling block only for the long modules (middle, outer) to help removing the heat generated by the detectors. The goal of the KB design is to have a single cooling block. The practical reason is to avoid a second cooling circuit on the disk thus reducing the material in the detector. The detectors and hybrid thermal paths have to be decoupled to avoid that the warmer hybrid dissipates part of its heat on the detectors. This concept, applied also in the baseline design, becomes more delicate when the heat paths have to reach the same cooling point. Different solutions have been studied and the final module design is shown in figure 1. The detectors are mounted on a tapered TPG[3] (Thermal Pyrolitc Graphite) spine that runs along the module to the cooling block. TPG is a pure-carbon material characterized by a high thermal conductivity xy-plane (1700 W/mK) and a low thermal conductivity in the orthogonal direction (8 W/mK). The hybrid is mounted on a CC (Carbon Carbon) bridge as in the barrel module; CC is a low mass "mono-dimensional" material, meaning that it has high thermally conductive fibers in one direction (700 W/mK) and low heat conductivity in the two orthogonal plane (35 W/mK). To decouple the different heat paths corresponding to the different TPG pieces, two L-shaped PEEK (PolyEtherEtherKetone) pieces have been inserted. Since the TPG is a soft material, to give mechanical robustness to the module two AlN facings enclose the TPG and the PEEK pieces. The legs of the bridge are then glued on this mechanical support.

The heat flow through the bond wires has been shown to be negligible in a very similar study performed on the barrel module (see reference [4]). A weak thermal coupling remains through the air gap between the bridge and the TPG spine. A compromise between a large gap inbetween hybrid and TPG and a small module envelop (necessary for the integration of the module on

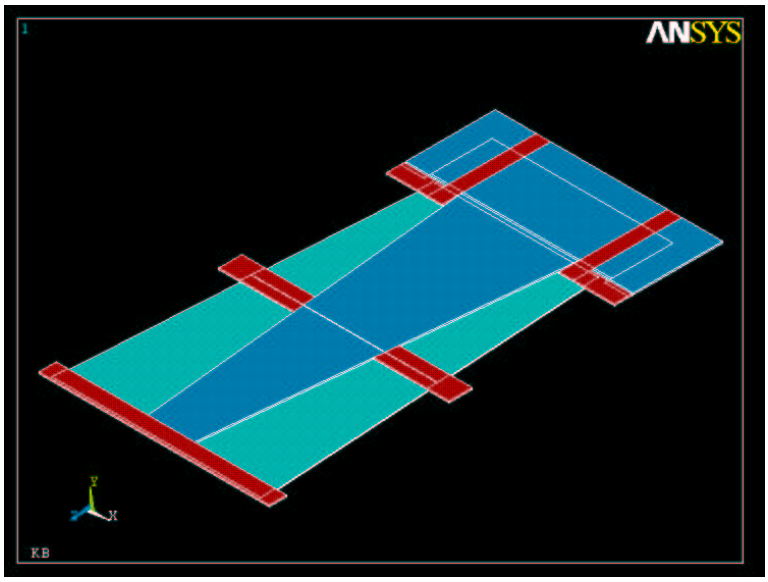

Fig. 1. Thermal design concept.

the disks) has been found.
The module will experience a heat load on the detectors coming from convection. Two contributions to the convective heat load on the detectors can be distinguished. The first is at the single module level: since the modules will be mounted vertically on the disks, when the hybrid is below the detectors they will experience a small load. (In our measurements the module has been mounted horizontally and kept in a flushing N_2 atmosphere to intentionally minimize this effect). The second one, which is the most relevant, comes from the warming effect of all the modules in the thermal enclosure. Since it is a global effect, a proper study requires to include the full SCT geometry [5], [6]. The module will also receive a heat load coming from the emission radiation. A safe estimate of 0.2 W per detector is usually assumed, including both convection and emission radiation. This becomes 0.8 W in the case of an outer module.

3.2 FEA model

The thermal simulations on the KB modules have been performed using ANSYS (version 5.7.1) [7]. This software is a commercial general purpose finite element analysis package that allows 3D simulations.
The thermal conductivities used in the simulations are listed in table 1. The detectors are modeled with 3D thermal-electrical elements. ANSYS allows to define the electrical resistivity of the material as a function of the temperature. In this way it is possible to include the leakage current temperature dependence, see equation (1), in the model. With this peculiarity it is possible to simulate the heat generation in the detectors and so analyze the runaway. The same thermal-electrical element allows to generate a constant 0.2 W per detectors to simulate the environmental heat load.

The hybrid and chips are replaced in this study with a single volume generating 3.5 W per side. The description of the temperature distribution on the hybrid is then not very accurate. The cooling block is fully simulated in the FEA model.

Material	Kx	Ky	Kz	Material	Kx	Ky	Kz
Air	0.024	0.024	0.024	Kapton	0.37	0.37	0.37
AlN	180	180	180	PEEK	0.92	0.92	0.92
Alumina	38	38	38	Silicon	136	136	136
Aluminum	190	190	190	Solder	50	50	50
CC	700	35	35	Thermal Grease	0.42	0.42	0.42
CuNi	29	29	29	TPG	1700	8	1700
Epoxy-glue	0.42	0.42	0.42	Vetronite	10	10	10

Table 1
Thermal conductivities in W/mK.

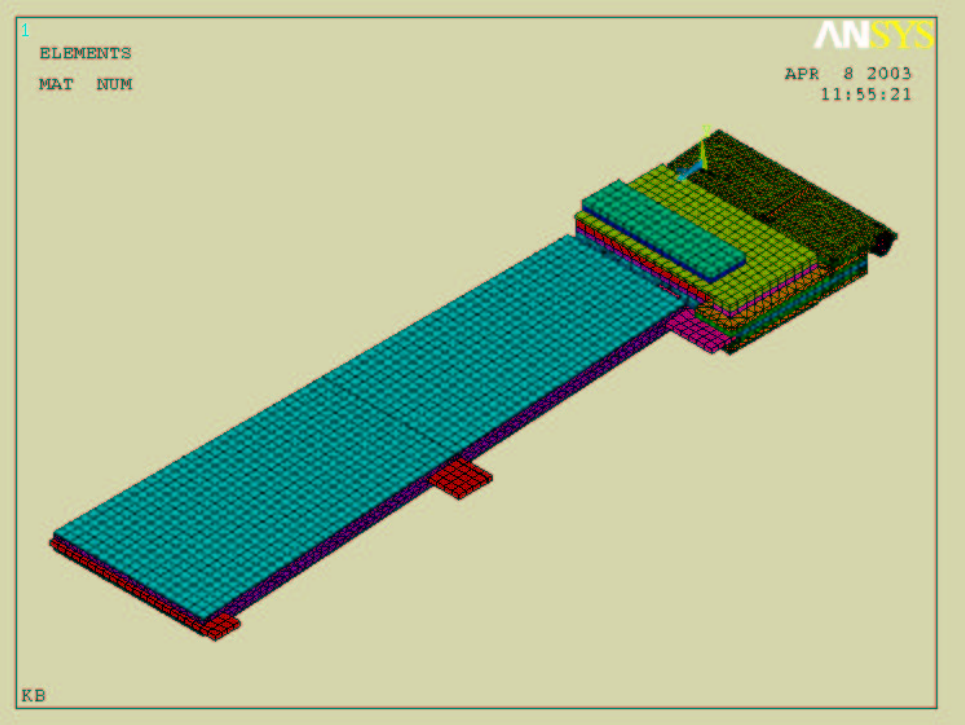

Fig. 2. FEA model.

The KB module has an adiabatic plane corresponding to its symmetry plane. Taking advantage of this it is possible to reduce the number of elements in the model to simulate only half of it.
The finite element subdivision (*mesh*) has been performed using hexahedron elements for all the materials but the glue layers and the cooling block volumes where tetrahedron elements has been used letting ANSYS finding the best possible mesh.
The stability of the mesh (temperatures independence from the finite elements size) has been accurately studied.
The boundary conditions to be set in this model are: the power dissipation in the chips, the power density in the detectors, the environmental heat load on the detectors and the coolant temperature.

The preliminary studies with this model aimed at finding the best materials to be used. Once a proper set of materials had been found, see table 1, a prototype module was assembled and irradiated. As shown in the following sections several thermal measurements were collected and then compared with the simulations. Once simulations agreed with the measurements, the model was used to predict the KB thermal performance in different cooling scenarios. Those results will be later presented (see section 5).

4 Thermal Measurements

Once the thermal design looked satisfactory in the light of the FEA studies, a prototype with those characteristics was built and tested.

4.1 Setup description

The setup used for the thermal measurements aimed at emulating in the laboratory the experimental environment where the module will have to operate. The relevant conditions to be controlled are the coolant temperature and the effect of convection and radiation on the detectors surface. The module used for these tests is the KB 100 which comes from a batch assembled at the university of Geneva. This module was irradiated at the 24 GeV PS proton beam up to the fluence of 3×10^{14}p/cm^2, annealed for one week at 25 °C and then stored in a freezer at about -20 °C . It was decided, for practical reasons, to use vetronite instead of PEEK in this prototype module and block. This increased the coupling between the detectors and hybrid thermal paths.
The module remained fully operative electrically all over the measurements. This means that high voltage was applied on the detectors and the readout electronics was powered and exercised via the SCT-DAQ. The module is mounted on a aluminum split cooling block (see figure 3) that allows to separate the hybrid and detector thermal paths. The split between the three pieces of Al will be made in PEEK, a plastic material with a low thermal conductivity. The material chosen for the pipe is CuNi. This low thermal conductivity material allows to have a large thermal resistance between the different portions of the cooling block, reducing the thermal couplings. On the other hand to have a low thermal resistance along the cooling path, the pipe thickness has been reduced to 70μm. For this first prototype the cooling pipe was glued onto the cooling block (thus the thermal resistance of the block is much higher than the real one where the glue will be substituted with solder) and the split has been realized with vetronite instead of PEEK (so a less effective split is achieved at the cooling block).
The coolant used in this test is a 60/40 mixture of water and ethanol. The temperature of the coolant is regulated by an Huber chiller [8]. The present design of the experiment cooling system is based on a C_3F_8 evaporative refrigerator cycle and it can reach temperatures between -30 °C and -15 °C . The HTC (Heat Transfer Coefficient) of the monophase liquid coolant is much lower than the evaporative one, so all the performed measurements have to be considered, with respect to this aspect,as conservative.
The convection and radiation conditions present in the experiment are much more difficult to emulate. In our tests the module is operated in a flushing nitrogen atmosphere and placed in

Fig. 3. Aluminum cooling block prototype ("split block design").

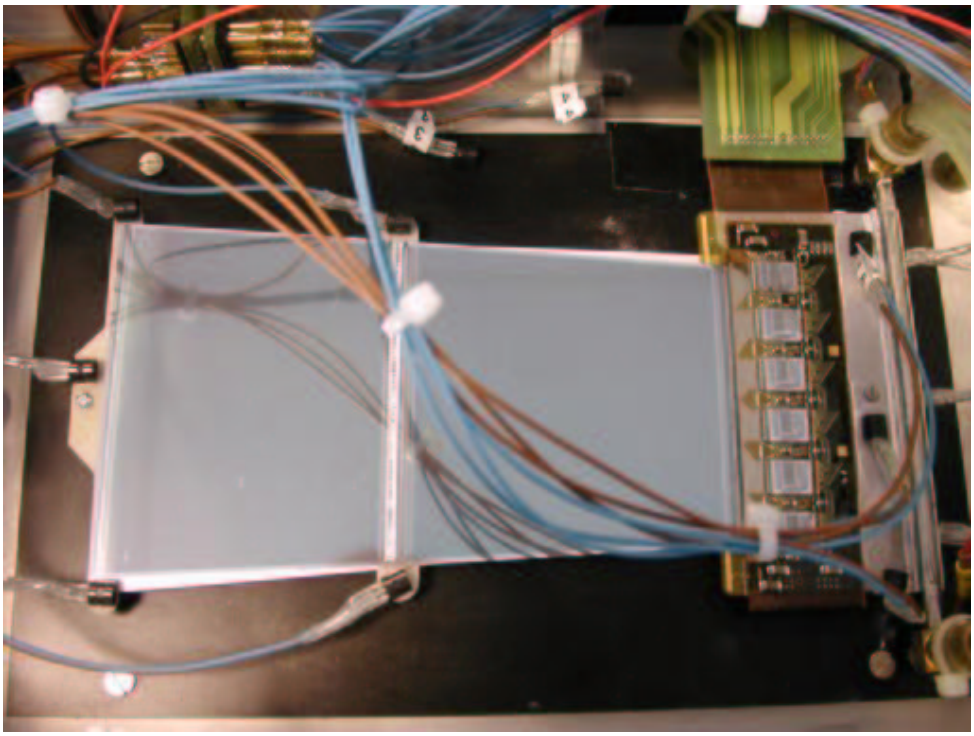

Fig. 4. Module mounted in the dedicated box with sensors glued at several location.

a dedicated test box (see figure 4) installed in a climate chamber. This feature allows to regulate the temperature of the box walls and, through a heat exchanger placed into the climate chamber, the temperature of the atmosphere in the box. Tuning the temperature of the climate chamber to the temperature of the detectors allows to reduce drastically the convection and radiation heat load on the detectors surface. This situation is then much easier to compare with simulations. [3]

The temperature regulation of the atmosphere inside the test box is also crucial to obtain precise temperature measurements with the sensors we used. The module and environment temperatures are measured with DS1820 [9] sensors glued at several critical points, see figure 5, and

[3] To remove any contribution from the atmosphere it would be better to test the module in vacuum but, due to practical reasons, this has not been possible.

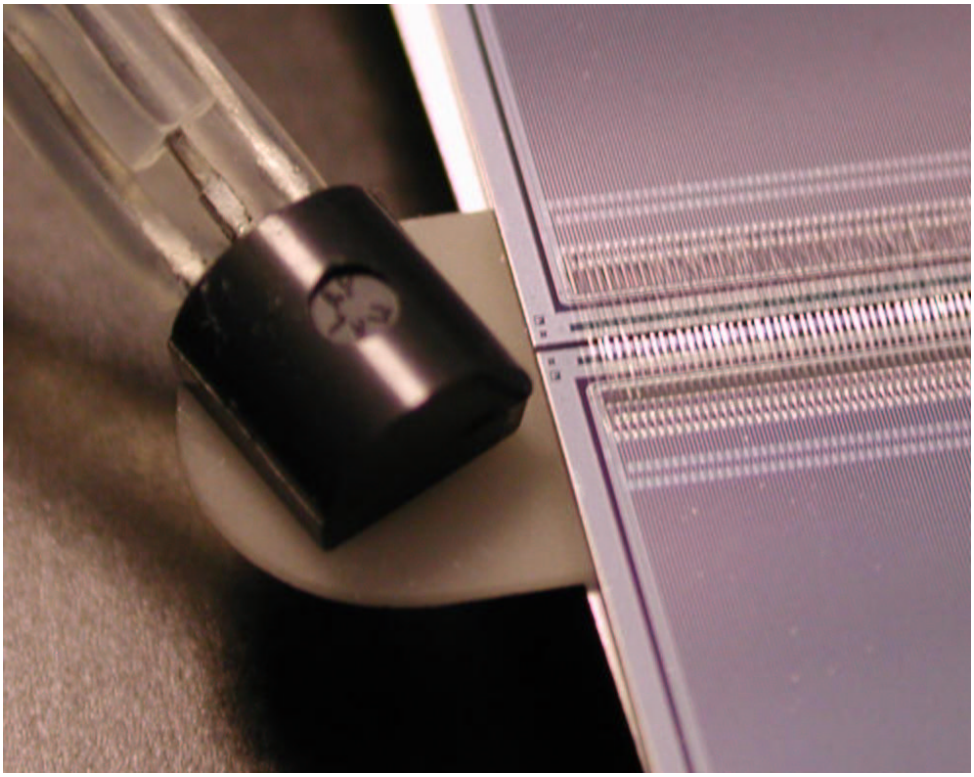

Fig. 5. Detail of a DS1820 sensors glued on an AlN wing.

readout with a dedicated LabView interface through a PointSix adapter [10].
The DS1820 sensors are cheap and the "infrastructure" needed to read them out is very much reduced. It is in fact possible to connect directly all the sensors to a PC serial port simply through a passive adapter. Since the sensors use a 1-wire protocol it is possible to short all the data bus together and at the same time address the sensors one by one, reducing the number of pins in the feed through of the sealed box.
An ideal sensor can read the temperature of the surface at which it is thermally grounded, regardless of the environment conditions surrounding it; none of the existing sensors allow this feature. To overcome this inconvenient we developed a specific procedure consisting of a two step calibration. First, the sensors are thermally grounded to a large block of aluminum placed in a climate chamber. Setting the block at different temperatures allows to check the linear response of the sensors over a wide range of temperatures. Those sensors appear to have an excellent linearity in the range of interest between -25 °C and +25 °C (see figure 6) Then a measurement of influence of the atmosphere temperature on the sensors read out is performed. The sensors are glued (with cyanolite) in their final position on the module (AlN wings) and in the box. The chiller temperature is set to a fixed low value (about -20 °C) and the atmosphere temperature is varied from -20 °C up to a about +30 °C . Since no power is injected in the module the temperature of the inlet, outlet, cooling block and facings are to a very good approximation at the same temperature of the coolant, while the detectors, due to their geometry (0.285 mm thick with a large area), change their temperature during this operation. For this reason the following calibration can only be applied to the sensors on the facings, on the cooling block and on the inlet/outlet. The sensors glued onto the AlN wings of the detectors *cannot* be treated in the same way and the adopted procedure is to tune the temperature of the atmosphere to the temperature of the detectors to eliminate the heat flow from the environment to the sensors and viceversa.
It is possible to observe from figure 7 that the measured value of the DS sensors varies sensibly,

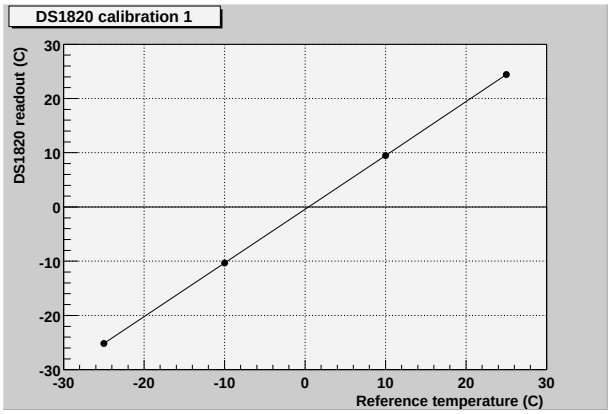

Fig. 6. Temperature values measured with a typical DS1820, plotted against the reference temperature.

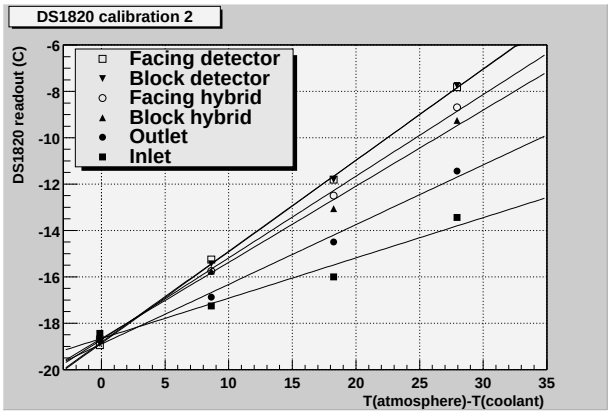

Fig. 7. Influence of the atmosphere temperature on the sensor readout value. In the plot the temperature read with the DS sensors is plotted against the temperature difference between the atmosphere and the real surface temperature assumed to be equal to the coolant temperature.

increasing the atmosphere temperature. The measured temperature, the real surface temperature and the atmosphere temperature can be related in the following way:

$$T_{read} = T_{surface} + k(T_{atm} - T_{surface}) \tag{2}$$

where k is the slope fitted from the previous plot. From this equation it is possible to work out the real temperature of the surface:

$$T_{surface} = (T_{read} - T_{atm})/(1 - k) \tag{3}$$

The measured k values are reported in table 2.

4.2 Thermal Measurements

The first and most delicate step in the preparation of the thermal measurements is to glue the temperature sensors on the module. In order to prove not to have damaged the detectors an

Position	k
inlet	0.17
outlet	0.26
block hybrid left	0.33
block detectors	0.39
block hybrid right	0.33
facing hybrid left	0.35
facing detectors	0.39
facing hybrid right	0.35

Table 2
Atmosphere influence correction factors

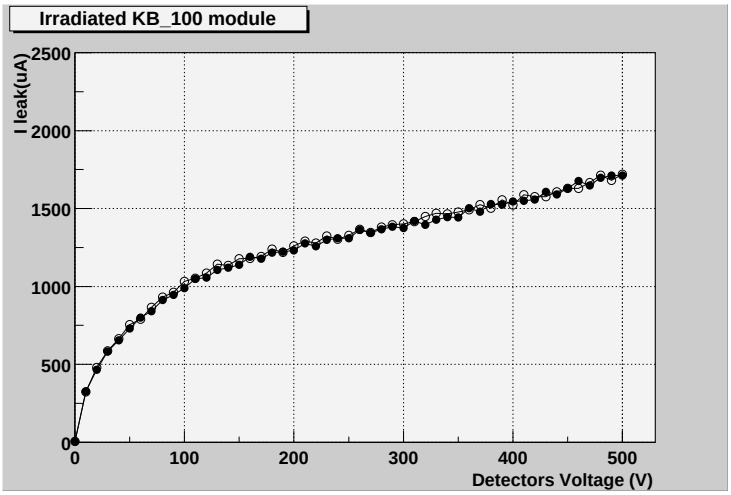

Fig. 8. IV-plot of the KB_100 module before (black dot) and after (white dot) gluing sensors on the module.

IV scan have been taken before and after gluing the sensors (see figure 8). As already shown in equation (1) the leakage current is a function of the temperature of the detectors. The essential parameter in that formula is *Egap*, corresponding to the energy gap for non irradiated silicon. The detectors have been irradiated with a fluence of 3×10^{14} protons/cm^2, so this parameter is now not simply the silicon energy gap but an effective value which takes into account the lattice defects and all the new energy levels created in the gap band during the irradiation. In figure 9 the Arrhenius method has been used to fit the leakage current formula and extract this parameter. The value found is 1.197 eV. In the same figure we show the leakage current measured at two different temperatures and then rescaled using the formula with the measured parameter. Irradiated modules are usually operated at 500V. When the module is properly cooled it draws a current of a few milliampere, so the current limit of 5mA at 500V of the SCT-HV power supply is appropriate for the usual electrical operations. When thermal tests are performed the module is pushed well above the optimal detector operating temperature and consequently much higher currents are involved. In order to overcome the current limitation of the SCT-HV, a bench power supply with an adjustable current limit is used. A fraction of the power delivered goes into the

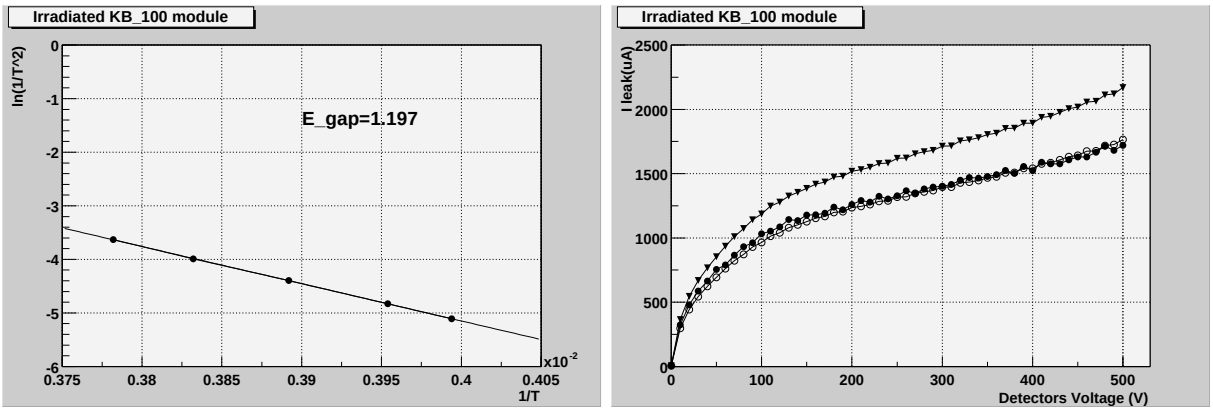

Fig. 9. LEFT: Effective energy gap measured changing the temperature on the detectors; RIGHT: IV-plot at different temperatures. Triangles show the IV-plot at -10.5 °C , black dots the measured curved at -12.5 °C and white dots the former rescaled according to the formula (1) using Egap=1.197 eV and a ΔT=2.0 degrees.

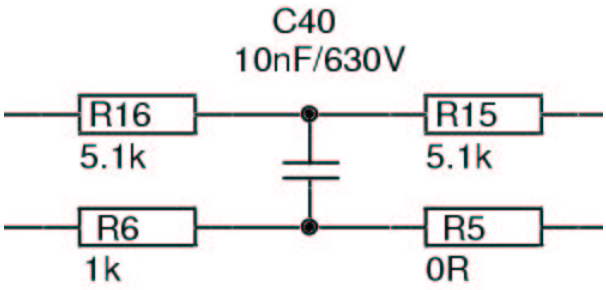

Fig. 10. High voltage filter on the hybrid.

detector power dissipation and the remaining is dissipated by the high voltage filter located on the hybrid showed in figure 10. The filter is equivalent to a series of resistors of 11.2 kΩ. The power dissipated on the hybrid is thus the sum of the readout chip power consumption and the high voltage filter contribution.

A thermal stability test has been performed with a coolant temperature of -15 °C and the atmosphere kept at -2 °C . The temperature difference between coolant and atmosphere is similar to what the modules will experience on average in the experiment where the coolant temperature is around -23 °C and the atmosphere -7 °C . The module, even in the already described conditions of poorly conducting cooling block and limited split in the detectors/hybrid thermal paths, has been demonstrated to be thermally stable.
After that a measurement of the thermal runaway has been performed at a coolant temperature of -10 °C . In this run the temperature of the flushing N_2 atmosphere has been tuned at each point to the detectors temperature to reduce the convection and radiation heat load on them and in order to have precise temperature measurements of the sensors on the AlN wings of the detectors.

Hybrid power (W)	Hybrid Temperature (°C)	V det supply (V)	V det (V)	Ileak (μA)	Detectors Power (W)	Power density ($\mu W/\mathrm{mm}^2$ at 0 °C at 0)
6.7	3/4	0	0	0	0	0
6.7	3/5	100	78	1969	0.15	15
6.8	3/5	200	164	3200	0.53	47
6.9	3/5	300	253	4120	1.05	83
7.0	5/5	400	340	5350	1.82	124
7.6	8/9	500	400	8960	3.58	172

Table 3
Module electrical parameters. In the hybrid temperature column, the temperature read by the two thermistors on the hybrid are reported.

4.2.1 Thermal stability test

A first test was performed to ensure that the module can be operated stably. In the experiment the coolant temperature will be around -23 °C and the nitrogen atmosphere, far from the convectional plume, is predicted to be around -7 °C with large variations between different module positions on the disk. In this run the coolant temperature is around -15 °C and the atmosphere is maintained at -2 °C all over the scan. In table 3 the power on the detectors and the power density normalized to 0 °C are shown.

The temperature on the hybrid is not constant because of the contribution coming from the additional power dissipated by the HV filter. In figure 11 the runaway plot is shown. The maximum and minimum temperature of the AlN wings are plotted against the power normalized to 0 °C . The normalization to 0 °C is the usual way to present the thermal runaway; in this way the plotted curve shows the point where the module reach the unstable condition as a vertical asymptote. In the same figure, the same phenomenon has been shown from a different point of view. When the module is operating in stable cooling conditions the variation of temperature across the detectors is negligible; when it approaches the runaway point, the corners of the detectors farther from the spine, will run warmer than those closer to it. The sensors glued on the AlN wings follow that behavior. The plotted temperature difference is between the warmest corner and the coolest wing between the two detectors. The coolest point of the detectors predicted with the simulations, is in the middle of the detector closer to the cooling block, so the plotted difference is underestimated, but nevertheless shows the expected behavior. As shown in figure 11, even with this poorly conductive cooling block and the less effective split of the thermal paths due to the use of the vetronite instead of PEEK, we were not able to approach the runaway point.
Considering the conditions achieved with the present setup it is possible to conclude that the module will not experience the thermal runaway when operated in the foreseen ATLAS-SCT environment.

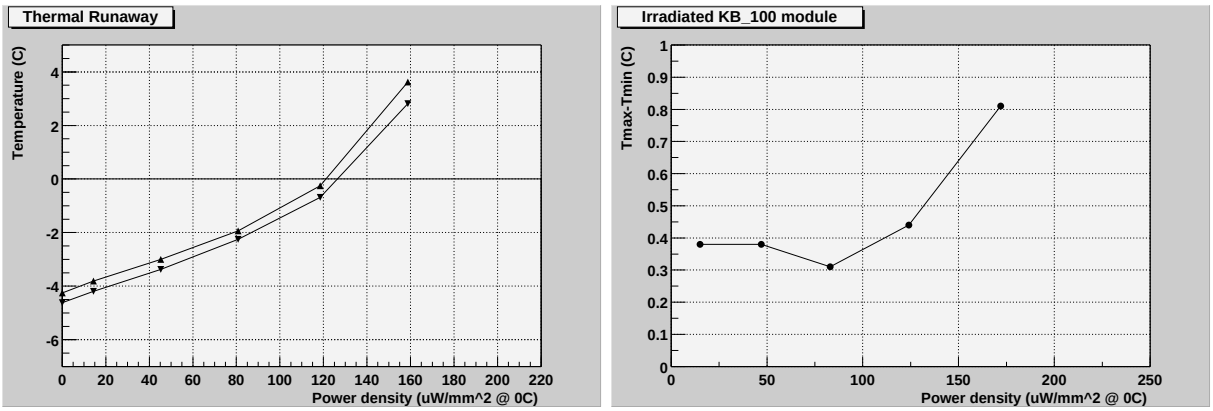

Fig. 11. LEFT: Runaway plot done with a coolant temperature of -15 °C and a fixed atmosphere temperature of -2 °C . With down triangles the coolest temperature measured on the wings, with up triangles the warmest one; RIGHT: Difference between the warmest and coolest temperature measured on the detectors.

Hybrid power (W)	Hybrid Temperature (°C)	V det supply (V)	V det (V)	Ileak (μA)	Detectors Power (W)	Power density ($\mu W/\mathrm{mm}^2$ at 0 °C at 0)
6.7	6/8	0	0	0	0	0
6.7	7/8	50	32	1568	0.05	4
6.8	7/8	100	70	2720	0.19	13
6.9	8/10	150	106	3840	0.41	26
7.0	9/10	200	142	5180	0.74	38
7.2	10/11	250	176	6600	1.16	52
8.7	13/14	300	191	9680	1.85	58

Table 4
Module electrical parameters. In the hybrid temperature column, the temperature read by the two thermistors on the hybrid are reported.

4.2.2 Runaway measurement

As demonstrated in the previous section the module can be operated stably in the ATLAS-SCT environment. To provoke the runaway the module has been operated at a coolant temperature of -10 °C . The temperature of the atmosphere has been tuned to the temperature of the detectors at each point of the scan. In table 4 the power dissipated by the detectors and the power density rescaled to 0 °C are shown.

The temperature difference between the detectors and the hybrid is always below 10 °C . In figure 12 the runaway plot is shown. From the presented measurements at a coolant temperature of -10 °C with the present poorly conducting cooling block and the non optimal thermal paths split, the runaway appears to be at about $65\mu W/\mathrm{mm}^2$ at 0 °C .

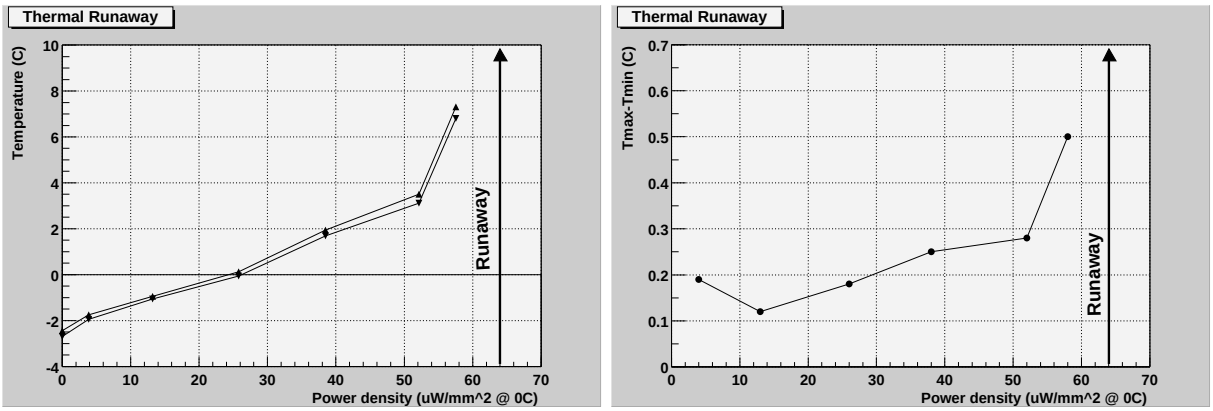

Fig. 12. LEFT: Runaway plot done with a coolant temperature of -10 °C . With down triangles the coolest temperature measured on the wings, with up triangles the warmest one; RIGHT: Difference between the warmest and coolest temperature measured on the detectors.

5 Simulations and measurements: comparison and predictions

The results coming from the FEA model previously discussed has been compared with the measurements.
As already seen, the measurements were performed with a liquid based chiller, the coolant being a mixture of ethanol and water. The heat transfer coefficient of this mixture to the CuNi pipe was not available, so it was decided to simplify the coolant-pipe interface description setting the inner wall of the cooling pipe to a fixed temperature. As already observed, the prototype module used for the measurements differs from the final one with one respect: the two L-shaped pieces separating the detectors from the hybrid thermal paths, have been produced in vetronite instead of PEEK. Vetronite has a thermal conductivity higher by an order of magnitude with respect to PEEK. This create a larger thermal coupling between hybrid and detectors. The cooling block is also slightly different with respect to the final one. The cooling pipe has been glued on the block instead of been properly soldered and the material used to split the different portions of the block is again vetronite instead of PEEK. The thickness of the thermal grease between the module and the block has been estimated to be around 200μm. Once these characteristics have been taken into account, only one parameter (the coolant temperature) has to be tuned to reproduce the measured situation. The measured inlet temperature in the box was about -10 °C ±1 °C and the value used in the simulations is -8.5 °C . In figure 13 the measured temperatures have been superimposed to the simulated thermal map. There is good agreement between the values measured on the detectors and the simulated values (the most accurately measured points and the most accurately modelled). The agreement is a bit worse on the hybrid probably because of the extreme simplification adopted in the FEA.
Once the coolant temperature has been tuned, the model has been used to predict the detector temperature at different power densities. Figure 14 shows that the agreement is within half a degree down to $26\mu W/\mathrm{mm}^2$ at 0 °C . At low powers the model prediction differs from the measured values by about one degree. This can be explained by the inaccuracy introduced using a fixed temperature on the inner wall of the cooling pipe instead of the heat transfer coefficient description of the coolant-pipe interface.
The runaway point one can extract from the simulations in these conditions is at about $75\mu W/\mathrm{mm}^2$ at 0 °C , in good agreement with the measured value. The FEA model allows us to understand the module and it can now be used as a tool to investigate the thermal performance in the

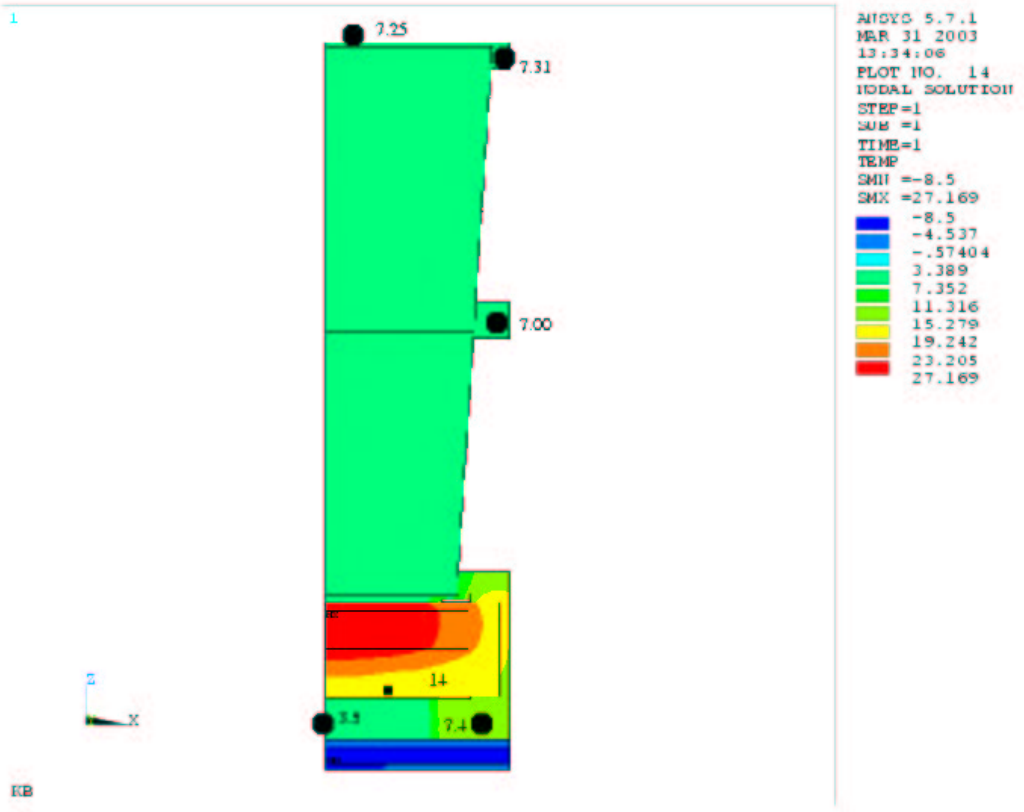

Fig. 13. Thermal map obtained with $58\mu W/\mathrm{mm}^2$ at 0 °C fixing the pipe inner wall temperature to -8.5 °C . The black dots represent the measured temperatures and the black rectangle represents the position of the thermistor on the hybrid surface.

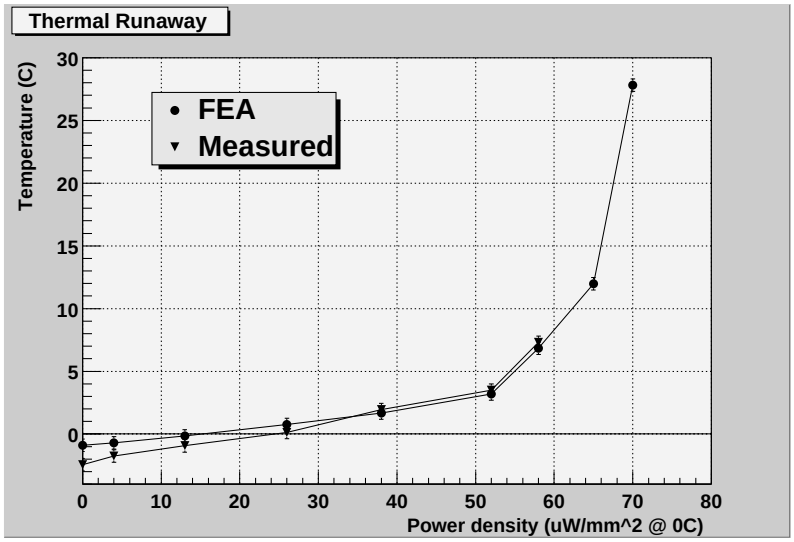

Fig. 14. Comparison between the simulated (dots) and the measured (triangles) runaway curves. (Maximal temperature of the detectors versus the detectors power density normalized to 0 °C).

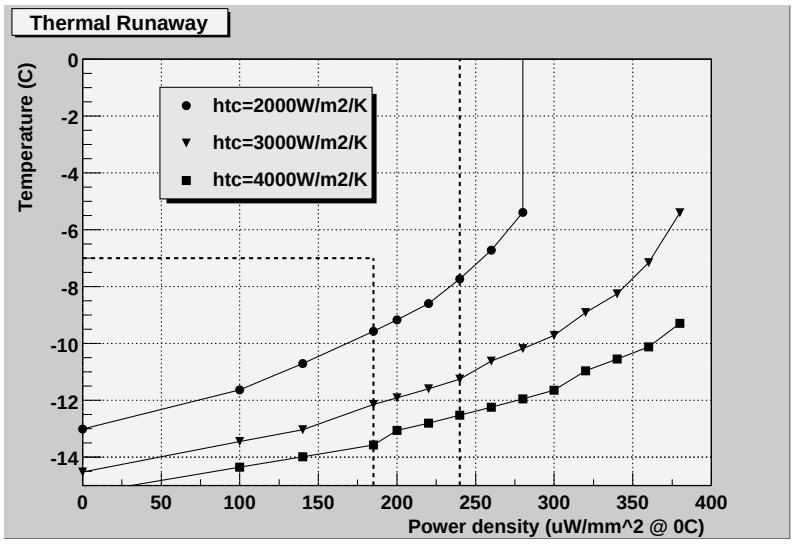

Fig. 15. Runaway plot using a coolant temperature of -20 °C for different heat transfer coefficients. (Maximal temperature of the detectors versus the detectors power density normalized to 0 °C). The dashed lines indicate the specifications: the detectors have to be cooler than -7 °C up to $185\mu W/\mathrm{mm}^2$ at 0 °C and the runaway must not occur below $240\mu W/\mathrm{mm}^2$ at 0 °C .

expected cooling conditions of the ATLAS-SCT.
As a first step the materials in the model for this prototype module and block have to changed to the one foreseen in the experiment: PEEK instead of vetronite and solder instead of glue on the cooling block. The grease between the module and the block has been fixed to a safe value of $\sim 100\mu$m.
Then the fixed temperature on the pipe inner wall, has to be substituted to the heat transfer coefficient description of the coolant-pipe interface. Recent measurements of the heat transfer coefficient [11] suggest a value around 3000 W/m^{2}K, but this measurement is affected by large uncertainties. In figure 15 the runaway plot is shown fixing the coolant temperature at -20 °C and three values of the heat transfer coefficient have been considered around the expected 3000 W/m^{2}K.
The runaway point is around $400\mu W/\mathrm{mm}^2$ at 0 °C considering a heat transfer coefficient of 3000 W/m^{2}K, but the module is still within the specification with a heat transfer coefficient of 2000 W/m^{2}K.

To simulate the heat load of 0.2 W per detector coming from convection and emission radiation, it has been decided to generate that extra-power in the detectors volumes taking advantage of the ANSYS "thermal elements". The results are reported in figure 16.
The module is still within the specifications with -20 °C coolant temperature and a heat transfer coefficient of 3000 W/m^{2}K, but it is out of specifications if the heat transfer coefficient is reduced to 2000 W/m^{2}K.
The final step of this analysis is to look for the coolant temperature needed to meet the specification with the different heat transfer coefficients. The results are shown in figure 17. The coolant temperature needed to meet the specification if the HTC is 2000 W/m^{2}K is -22 °C while it can be raised up to -18 °C if the HTC is 4000 W/m^{2}K. In figure 18 the thermal map expected with a coolant temperature of -20 °C and an HTC of 3000 W/m^{2}K is shown. In this condition the temperature differences between different parts of the detectors are listed in table 5.

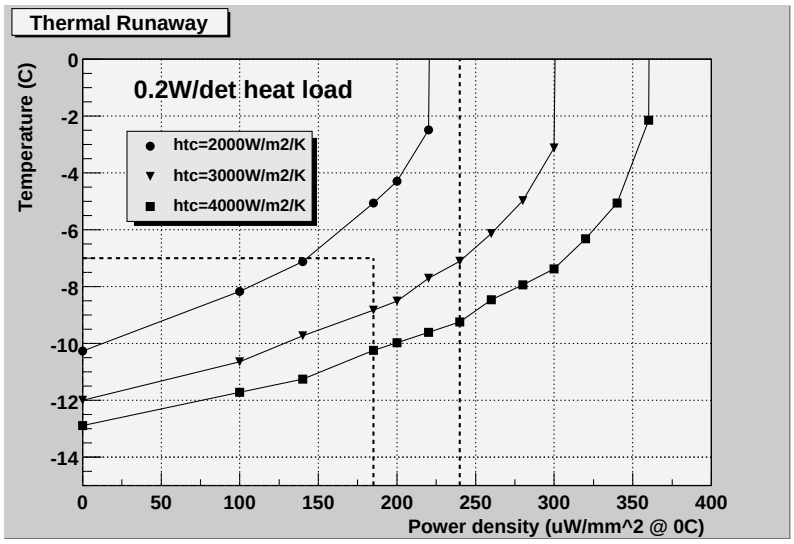

Fig. 16. Runaway plot using a coolant temperature of -20 °C for different heat transfer coefficients when the heat load of 0.2W per detector coming from convection and emission radiation is simulated. (Maximal temperature of the detectors versus the detectors power density normalized to 0 °C). The dashed lines indicate the specifications: the detectors have to be cooler than -7 °C up to $185\mu W/\mathrm{mm}^2$ at 0 °C and the runaway must not occur below $240\mu W/\mathrm{mm}^2$ at 0 °C .

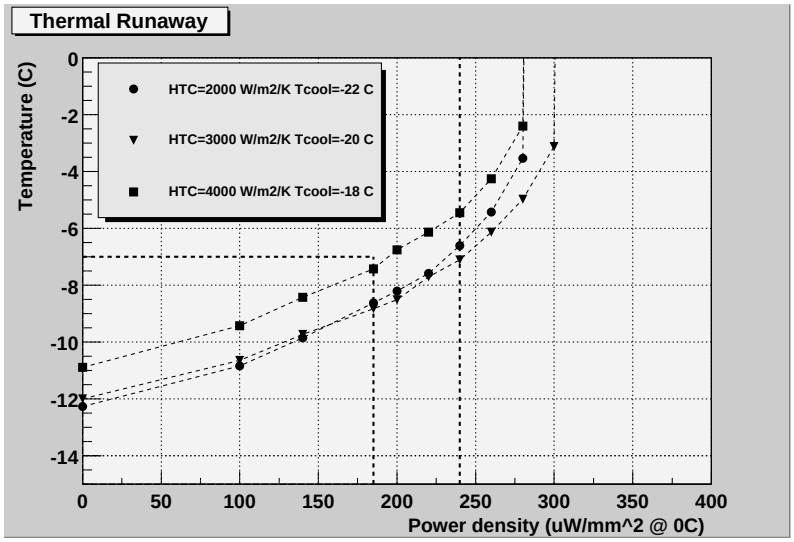

Fig. 17. Runaway plots obtained tuning the coolant temperature in order to meet the specifications for different heat transfer coefficients. The heat load of 0.2W per detector coming from convection is simulated. The dashed lines indicate the specifications: the detectors have to be cooler than -7 °C up to $185\mu W/\mathrm{mm}^2$ at 0 °C and the runaway must not occur below $240\mu W/\mathrm{mm}^2$ at 0 °C .

6 Conclusions

The thermal design of the KB ATLAS-SCT end-cap module has been developed and refined with a FEA model in order to meet the operational thermal specifications. A prototype module has been assembled and irradiated up to a fluence of $3 \times 10^{14}\mathrm{p/cm}^2$ (24 GeV protons). The thermal

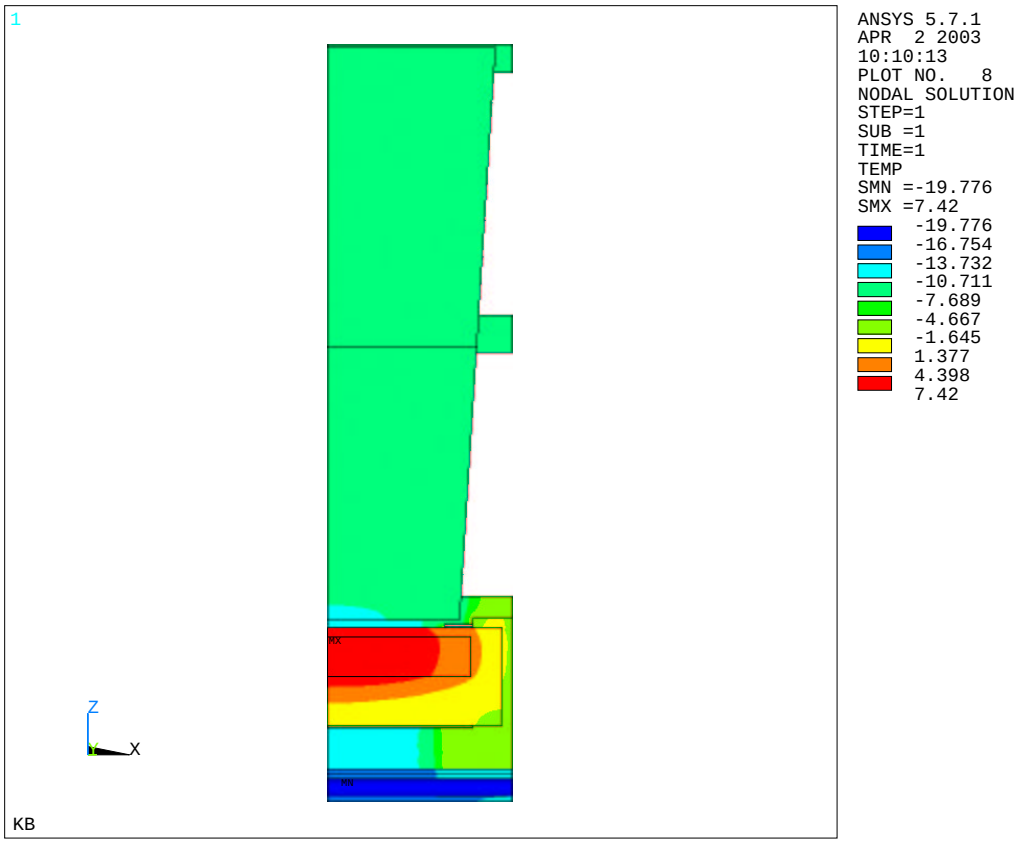

Fig. 18. Thermal map obtained with a power density of $185\mu W/\mathrm{mm}^2$ at 0 °C , coolant temperature = -20 °C , heat transfer coefficient = 3000 $\mathrm{W/m^2K}$ and including a heat load of 0.2 W per detector simulating the heat load coming from convection and emission radiation in the SCT.

Δ(Tcoolant - Tmax det)	11
Δ(Tcool - Tmax hyb)	27
Δ(Tcool - Thyb)	20
Δ(Tmax - Tmax det)	16
Δ(Thyb - Tmax det)	9

Table 5
Temperature differences as predicted by the FEA with a power density of $185\mu W/\mathrm{mm}^2$ at 0 °C , coolant temperature = -20 °C , heat transfer coefficient = 3000 $\mathrm{W/m^2K}$ and including a heat load of 0.2 W per detector simulating the heat load coming from convection and emission radiation in the SCT.

performance of the module has been measured in a controlled environment. The FEA analysis of the measured data has been used to predict the module thermal performance in a realistic SCT cooling scenario. Different heat transfer coefficients have been considered to overcome the present uncertainties on the exact value.
The module mounted on the proposed cooling block easily meets the thermal specification at

a coolant temperature of -20 °C assuming a heat transfer coefficient of 3000 W/m^2K and an additional heat load of 0.2 W per detector representing the effect of the convection and emission radiation on the detectors.

References

[1] Snow, S., Thermal and Mechanical Specifications and Expected Performance of the Forward SCT Module. *ATL-IS-EN-0007* (2002)

[2] M. D'Onofrio, et al., Electrical test results from ATLAS-SCT end-cap modules. (2003)

[3] Moore, A.V., "Highly Oriented Pyrolitc Graphite and its Intercalation Compounds" *Chemistry and Physics of Carbon, v.17, pp233-304* (1981)

[4] Kondo, T., *et al.* "Thermal simulation of ATLAS barrel SCT modules -I" *INDET-NO-202* (1998)

[5] Fowler, R.F. CFD Simulations of convection in the Atlas Forward Silicon Tracker.

`http://hepwww.rl.ac.uk/Atlas-SCT/engineering/ec\_fdr/misc/convection\_v2.pdf`

[6] Thompson, R, et al Measurements of convection between the disks of the ATLAS SCT end cap.

`http://www.hep.man.ac.uk/groups/atlas/TM/CONVECTION8.DOC`

[7] ANSYS, Inc.

`http://www.ansys.com`

[8] Huber Chiller

`http://www.ctpbuchi.com/heating\_cooling\_overview.htm`

[9] DS1820 Temperature sensor

`http://www.maxim-ic.com/quick\_view2.cfm/qv\_pk/3021/ln/en`

`http:/pdfserv.maxim-ic.com/arpdf/DS1820-DS1820S.pdf`

[10] Point six: RS232 to 1-Wire adapter

`http://www.pointsix.com/cgi-bin/PointSix.cgi?IHosts&DS9097U-K`

[11] Snow, S. et al The C_3F_8 evaporative heat transfer coefficient.

`http://www.hep.man.ac.uk/groups/atlas/TM/RALhtc.doc`